JEM Journal of Experimental Medicine

BRIEF DEFINITIVE REPORT

Ki67 deficiency impedes chromatin accessibility and BCR gene rearrangement

Zhoujie Ding[1*], Maree Hagan[2*], Feng Yan[3], Nick W.Y. Schroer[1], Jack Polmear[4,5], Kim L. Good-Jacobson[4,5], Alexandra R. Dvorscek[1], Catherine Pitt[1], Kristy O'Donnell[1], Stephen L. Nutt[6,7], Dimitra Zotos[1], Craig McKenzie[1], Danika L. Hill[1], Marcus J. Robinson[1], Isaak Quast[1], Frank Koentgen[2**], and David M. Tarlinton[1**]

The proliferation marker Ki67 has been attributed critical functions in maintaining mitotic chromosome morphology and heterochromatin organization during the cell cycle, indicating a potential role in developmental processes requiring rigid cell-cycle control. Here, we discovered that despite normal fecundity and organogenesis, germline deficiency in Ki67 resulted in substantial defects specifically in peripheral B and T lymphocytes. This was not due to impaired cell proliferation but rather to early lymphopoiesis at specific stages where antigen–receptor gene rearrangements occurred. We identified that Ki67 was required for normal global chromatin accessibility involving regulatory regions of genes critical for checkpoint stages in B cell lymphopoiesis. In line with this, mRNA expression of *Rag1* was diminished and gene rearrangement was less efficient in the absence of Ki67. Transgenes encoding productively rearranged immunoglobulin heavy and light chains complemented Ki67 deficiency, completely rescuing early B cell development. Collectively, these results identify a unique contribution from Ki67 to somatic antigen–receptor gene rearrangement during lymphopoiesis.

Introduction

Ki67 is a nuclear protein used extensively as a marker of cell proliferation (Gerdes et al., 1983). It is expressed throughout the cell cycle and is highly conserved in vertebrates and only downregulated when cells exit the cell cycle and enter G0 phase (quiescence) (Miller et al., 2018; Sobecki et al., 2017). Despite its widespread use, only recently have the functions of Ki67 started to be revealed. In cultured human cell lines, Ki67 remains in close contact with chromatin and chromosomes during the cell cycle, functioning as a "surfactant" to maintain proper mitotic chromosome morphology and promote chromosome clustering in cells exiting mitosis (Cuylen et al., 2016; Cuylen-Haering et al., 2020; Garwain et al., 2021). Importantly, Ki67 binds the heterochromatin protein 1 family (Scholzen et al., 2002) and is necessary also for normal heterochromatin organization during interphase (Sobecki et al., 2016). These properties indicate that Ki67 may be essential for biological processes requiring tight control of the cell cycle. Somewhat remarkably, the gross development of whole animals with partial knockdown of Ki67 is normal (Sobecki et al., 2016). However, it remains unclear whether Ki67 plays a vital role in vivo, as no detailed characterization of complete Ki67-knockout animals has been reported.

Lymphopoiesis is one of the developmental processes that depend on rigid regulation of the cell cycle (Mandal et al., 2009; von Freeden-Jeffry et al., 1997). During lymphocyte development, stages of gene rearrangement are interspersed by bursts of precursor cell proliferation and differentiation, driven by a combination of productive antigen–receptor rearrangement mediated by the recombination-activating gene (RAG) 1 and 2 complex and cytokines (Melchers, 2015). Early B cell development in bone marrow (BM) comprises sequential stages separated by checkpoints that assess variable (V), diversity (D), and/or joining (J) gene segment rearrangement status at the immunoglobulin (Ig) heavy then light chain loci (Hardy and Hayakawa, 2001). A parallel process occurs in T cells, resulting in the formation of a population with diverse T cell receptors at the $CD4^+CD8^+$ double positive (DP) thymocyte stage of development (Germain, 2002). Failure, or even inefficiency, in any of the specific stages of antigen–receptor rearrangement has profound effects on lymphocyte development ranging from

[1]Department of Immunology, Central Clinical School, Monash University, Melbourne, Australia; [2]Ozgene Pty Ltd., Bentley, Australia; [3]Bioinformatics Division, Walter and Eliza Hall Institute of Medical Research, Parkville, Australia; [4]Department of Biochemistry and Molecular Biology, Monash University, Clayton, Australia; [5]Immunity Program, Biomedicine Discovery Institute, Monash University, Clayton, Australia; [6]Immunology Division, Walter and Eliza Hall Institute of Medical Research, Parkville, Australia; [7]Department of Medical Biology, University of Melbourne, Parkville, Australia.

*Z. Ding and M. Hagan contributed equally to this paper; **F. Koentgen and D.M. Tarlinton contributed equally to this paper. Correspondence to Zhoujie Ding: zhoujie.ding@monash.edu; David M. Tarlinton: david.tarlinton@monash.edu.

complete block through to restrictions in lymphocyte number and repertoire (Csomos et al., 2022; Ng et al., 2020; Nutt et al., 1997).

To investigate physiological roles for Ki67 in vivo, we generated a germline Ki67-knockout (*Mki67*$^{-/-}$) mouse strain. Although animal development was largely normal in the absence of Ki67, we identified that early lymphocyte development was significantly impaired, resulting in a specific reduction in mature lymphocytes in peripheral lymphoid organs. Ki67 was required for maintaining global chromatin accessibility in B cell precursors, particularly at stages where antigen–receptor gene rearrangements occur. Importantly, we found that Ki67 deficiency impaired V(D)J gene rearrangement, and this developmental defect could be rectified by the provision of transgenes encoding pre-rearranged heavy (H) and light (L) chains. Collectively, this study reveals a distinct and previously unknown requirement for Ki67 in normal lymphocyte development.

Results and discussion

Ki67-deficient mice are largely normal except for selective reductions in B and T lymphocytes

To investigate the cellular function of Ki67 in vivo, mice with germline deficiency in Ki67 were generated via deletion of exon 4 of the *Mki67* gene (*Mki67*$^{-/-}$) (Fig. S1, A–C) creating a frameshift that disrupted the translation of the chromatin-binding domains of the Ki67 protein (Cuylen et al., 2016; MacCallum and Hall, 2000) (Fig. S1 D). Successful deletion of exon 4 was confirmed by quantitative PCR (qPCR) from tissue biopsies of *Mki67*$^{-/-}$ mice (Fig. S1 E), while the absence of Ki67 protein was confirmed by western blot and flow cytometry (Fig. S1, F and G). In agreement with previous studies that showed normal animal development when Ki67 was diminished (Sobecki et al., 2016), *Mki67*$^{-/-}$ mice had normal gross organ development (Fig. 1 A) and litter sizes (Fig. 1 B). No significant alterations in tissue morphology were found in histological examination of sections from skin, lung, liver, small intestine, BM, thymus, and spleen of *Mki67*$^{-/-}$ mice (Fig. S1 H). A small but significant decrease in body weight of *Mki67*$^{-/-}$ mice compared with WT mice was observed throughout life (Fig. 1 C), although lifespan itself was unaffected (Fig. 1 D). Thus, whole organism Ki67 deficiency has minimal effect on survival, reproduction, and organ development under specific pathogen–free conditions, confirming and extending previous results (Sobecki et al., 2016).

We next examined immune cell composition in the spleen of *Mki67*$^{-/-}$ mice, which revealed an average 2.5-fold decrease in total splenocyte number compared to WT (Fig. 1 E). This in turn was due to a specific and significant impairment in the accumulation of B and T cell populations, as the representation of other white blood cell lineages assessed here (natural killer cells, dendritic cells, eosinophils, neutrophils, and monocytes) was unaffected (Fig. 1, F and G). The reduction in lymphocytes was not due to the impaired proliferation potential of mature *Mki67*$^{-/-}$ cells (Fig. 1, H and I), which was in line with previous studies showing cell proliferation to be largely unaffected by Ki67 deficiency (Cuylen et al., 2016; Mrouj et al., 2021; Sobecki et al., 2016). Thus, from both direct measurements here and inferred by the largely normal development in Ki67-deficient animals from our data and observed previously (Sobecki et al., 2016), Ki67 is not required for cell proliferation. However, intriguingly, Ki67 deficiency selectively reduces peripheral B and T lymphocyte representation.

Ki67 deficiency affects early lymphocyte development

To determine the basis of the reduced number of mature lymphocytes in the spleen when Ki67 was absent, we analyzed early B and T cell development in the BM and thymus, respectively. The total number of total BM cells, Lineage$^-$Sca-1$^-$Kit$^+$ (LK) cells, and Lineage$^-$Sca-1$^+$Kit$^+$ (LSK) stem cells was not altered by the absence of Ki67 (Fig. 2, A–C); however, B220$^+$ B lineage cells in the BM were significantly decreased (Fig. 2, B and C). Resolving the early stages of B cell development (Fig. 2 D) revealed that the number of large pre-B, small pre-B, and immature B cells was decreased approximately two-, nine-, and seven-fold, respectively, in the absence of Ki67 (Fig. 2 E). Using a differentiation index to measure progress across each developmental step revealed that impaired representation first occurred at the pre-pro-B to pro-B stage (Fig. 2 F). Similarly, the total number of thymocytes was decreased in the absence of Ki67 (Fig. S2 A) with the deficits in T cell development occurring predominantly at the CD4$^-$CD8$^-$ double negative (DN) 3 to DN4 and DN4 to CD4$^+$CD8$^+$ DP stages (Fig. S2, B–D).

To determine whether impaired lymphocyte development in the absence of Ki67 was intrinsic to lymphocyte progenitors, we reconstituted lethally irradiated CD45.1 recipients with a mixture of BM containing either 90% CD45.2 WT and 10% CD45.1 WT BM cells or 90% CD45.2 *Mki67*$^{-/-}$ and 10% CD45.1 WT BM cells (Fig. S2 E). 6 wk after reconstitution, the cellular composition of the BM and thymi of the recipients was analyzed. In line with the findings in intact *Mki67*$^{-/-}$ mice, significant impairments in early B (Fig. S2, F and G) and T cell development (Fig. S2, H and I) were observed among cells derived from CD45.2 *Mki67*$^{-/-}$ BM cells in the chimeras. Together, these data show that Ki67 deficiency intrinsically and specifically impairs the development of B and T lymphocytes at early stages.

Ki67 sustains normal chromatin state at specific B cell developmental stages

The partial blockages in early lymphocyte development in the absence of Ki67 coinciding with stages where antigen–receptor gene rearrangement occurred led us to hypothesize that Ki67 was required for this lymphocyte-specific process. As Ki67 is known to be an important contributor to chromatin organization (Sobecki et al., 2016; van Schaik et al., 2022) and that chromatin configuration directly regulates the process of antigen–receptor gene rearrangement (Cherry and Baltimore, 1999; Lion et al., 2020; Stanhope-Baker et al., 1996), we first assessed whether Ki67 deficiency affected chromatin accessibility states, focusing on B cell progenitors. We performed an assay for transposase-accessible chromatin sequencing (ATAC-seq) on sorted pre-pro-B, pro-B, and small pre-B cells, representing the developmental stages preceding V(D)J rearrangement, where Ig heavy chain rearrangement occurs, and where Ig light chain rearrangement occurs, respectively.

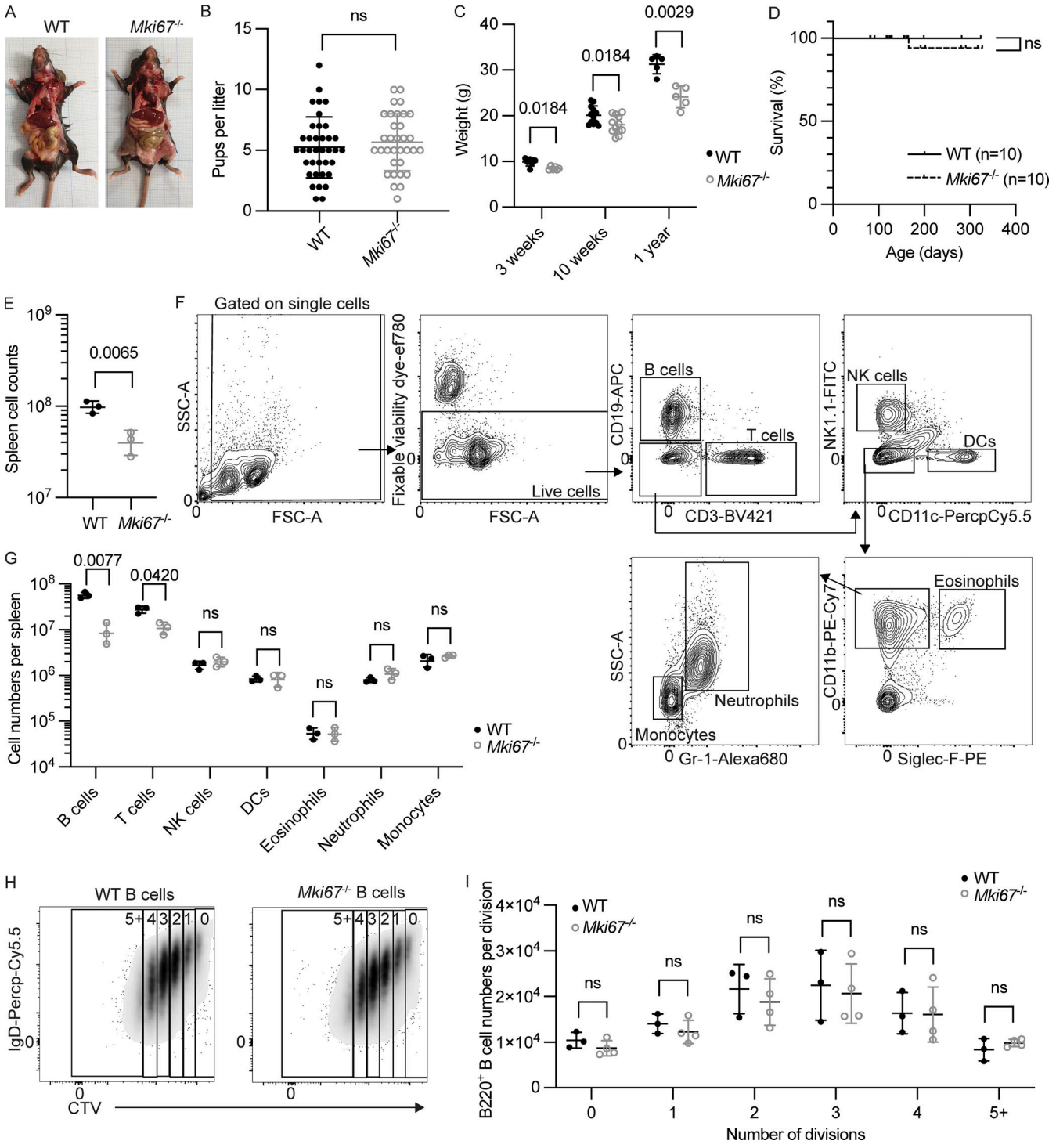

Figure 1. ***Mki67*$^{-/-}$ mice have specific impairment in lymphocyte-lineage compartment in the spleen despite normal reproduction, organogenesis, and mature lymphocyte cell proliferation. (A)** Representative photos showing overall organ morphology of WT and *Mki67*$^{-/-}$ mice. **(B)** Litter sizes of the WT (37 litters from 24 female breeders) and *Mki67*$^{-/-}$ mice (33 litters from 12 female breeders). **(C)** Body weights of WT and *Mki67*$^{-/-}$ mice at 3 wk (n = 6 for each genotype), 10 wk (n = 12 for each genotype), and 1 year (n = 5 for each genotype) of age. **(D)** Survival curves of WT (n = 10) and *Mki67*$^{-/-}$ (n = 10) mice within 1 year of age. **(E)** Total splenocyte counts in WT (n = 3) and *Mki67*$^{-/-}$ (n = 3) mice. **(F)** Gating strategy of the lymphoid and myeloid cell subsets in the spleen. **(G)** Quantification of the B, T, and myeloid cell subset cell numbers in the spleen of WT (n = 3) and *Mki67*$^{-/-}$ (n = 3) mice. NK, natural killer; DC, dendritic cell. **(H)** Gating strategy of CTV dilution peaks in B cell cultures stimulated by anti-CD40 and IL-4. **(I)** Quantification of cell division in cultures of mature B cell from WT (n = 3) and *Mki67*$^{-/-}$ (n = 4) mice. Data in E–G are representative of three independent experiments and in H and I are representative of two independent experiments. Statistical differences in B and E were determined by two-tailed unpaired t test, in C, G, and I by multiple unpaired t tests (corrected for multiple comparisons using the Holm–Sidak method), and in D by Kaplan–Meier test. Adjusted P values are shown. ns, P > 0.05.

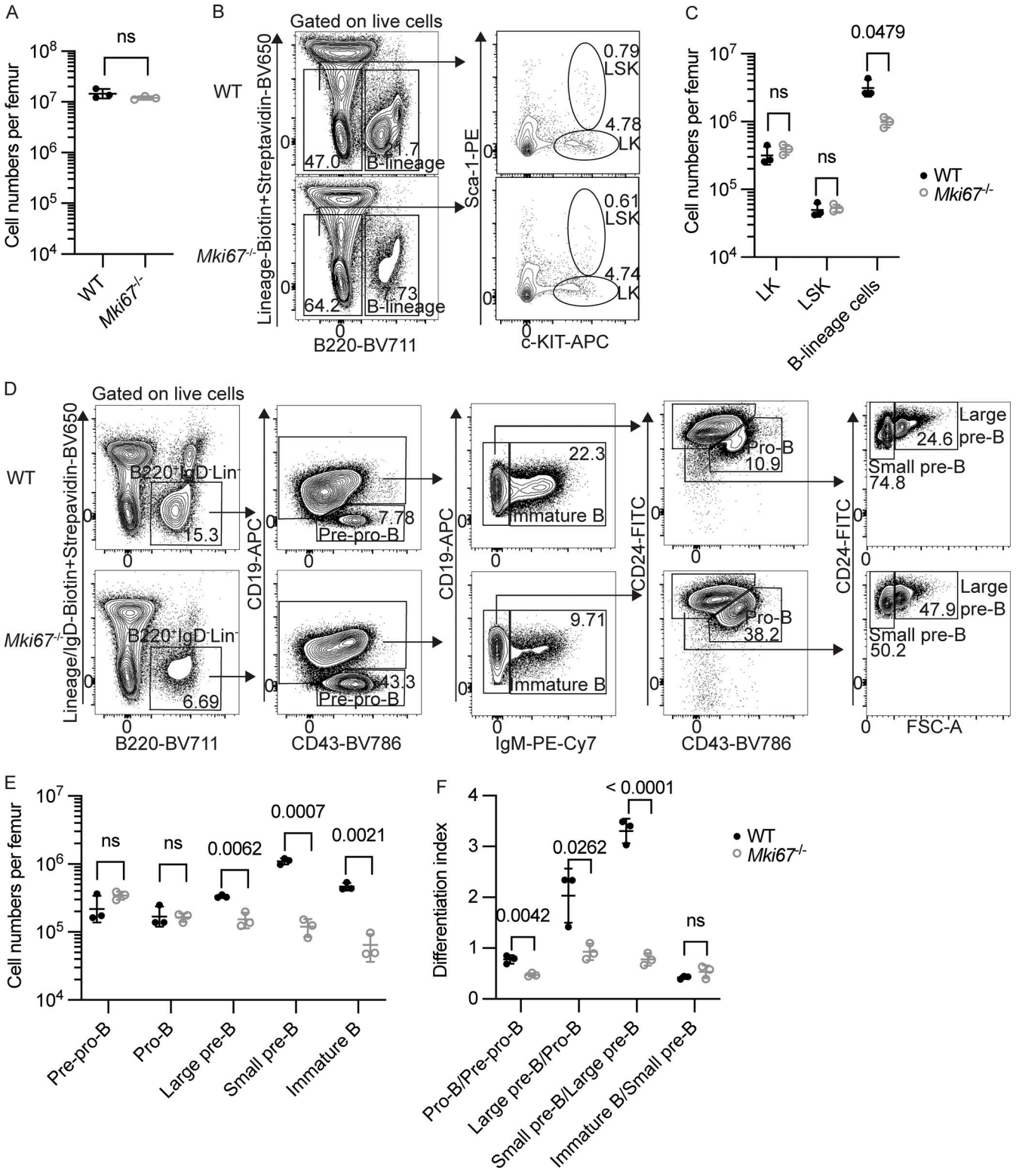

Figure 2. **Ki67 deficiency results in significant defects in early B cell development. (A)** Total BM cell counts of WT (n = 3) and *Mki67*$^{-/-}$ (n = 3) mice. **(B)** Gating strategy of LK, LSK, and B-lineage cells. Representative percentages of the gated population of the parental gate are shown. **(C)** Quantification of cell numbers of LK, LSK, and B220^{+} B-lineage cells per femur in WT (n = 3) and *Mki67*$^{-/-}$ (n = 3) mice. **(D)** Gating strategy of B cell progenitors at pre-pro-B, pro-B, large pre-B, small pre-B, and immature B cell stage. Representative percentages of the gated populations of the parental gate are shown. **(E)** Quantification of cell numbers of B cell progenitors at each developmental stage per femur in WT (n = 3) and *Mki67*$^{-/-}$ (n = 3) mice. **(F)** Differentiation indexes calculated as the cell number of a later B cell developmental stage divided by that of the former stage in WT (n = 3) and *Mki67*$^{-/-}$ (n = 3) mice. Data in A, D, E, and F are representative of five independent experiments and in B and C are representative of two independent experiments. Statistical differences in A were determined by two-tailed unpaired t test, and in C, E, and F by multiple unpaired t tests (corrected for multiple comparisons using the Holm–Sidak method). Adjusted P values are shown. ns, P > 0.05.

All the accessible regions present in *Mki67*$^{-/-}$ and WT cells were analyzed and principal component analysis (PCA) was performed for all populations from both genotypes. We found that the samples clustered according to their cell types with the first two components (PC1 = 53.59% and PC2 = 20.23%; Fig. 3 A), reflecting cell type–specific chromatin states of the B cell progenitors as previously shown (Boya et al., 2017). When the dynamics of chromatin states were followed from pre-pro-B to pro-B and from pro-B to small pre-B stage, about 85% and 70% of the total peaks identified, respectively, followed the same trend when comparing the WT and *Mki67*$^{-/-}$ conditions (Fig. 3 B), indicating a partial impact of Ki67 deficiency on the dynamics of chromatin configuration during B cell development. When PC3 was examined, we found that pro-B and small pre-B cells were well separated by their genotype (PC3 = 3.09%), whereas samples of pre-pro-B cells were not (Fig. 3 C). Indeed, substantial differences in chromatin accessibility were identified in pro-B and small pre-B cells depending on Ki67 sufficiency whereas minimal changes were observed in *Mki67*$^{-/-}$ versus WT pre-pro-B cells (Fig. 3 D). The systemic nature of the changes to chromatin accessibility due to the absence of Ki67 in pro-B and small pre-B cells was reflected by alterations being distributed along the lengths of all chromosomes (Fig. 3 E).

To investigate whether the altered chromatin configuration in *Mki67*$^{-/-}$ cells affected genes important for lymphocyte development, we performed gene ontology (GO) analysis on the differentially accessible regions (DARs) that were consistently less accessible in *Mki67*$^{-/-}$ pro-B and small pre-B cells. There were 8,436 less accessible regions in the *Mki67*$^{-/-}$ pro-B cells that corresponded to 6,330 uniquely assigned genes and 2,289 less accessible regions in the *Mki67*$^{-/-}$ small pre-B cells that corresponded to 1,727 uniquely assigned genes (Fig. 3 F). Among the uniquely assigned genes, 1,184 were in common to both cell types (Fig. 3 F), of which 1,008 were annotated using the GO term tool PANTHER (Thomas et al., 2022) (Fig. 3 G). GO term GO:0030154 (cell differentiation) was among the top 10 enriched GO terms (Fig. 3 G and Table S1). Collectively, these data demonstrate that Ki67 deficiency results in genome-wide chromatin accessibility changes at stages of B cell development where V(D)J rearrangement occurs.

Ki67 is required for normal *Rag1* expression and receptor gene rearrangement

Although chromatin accessibility at the *Igh* and *Igκ* loci was largely unchanged in the absence of Ki67 (Fig. S3, A and B), we identified significantly decreased accessibility at a region of the *Rag* locus in *Mki67*$^{-/-}$ pro-B and small pre-B cells annotated as a putative enhancer by the Immunological Genome Project (ImmGen) database (Yoshida et al., 2019) (Fig. 4, A and B). An accessibility peak of this region at the *Rag* locus was also detected in DN3 thymocytes according to the ImmGen database but largely absent in cells where *Rag1/2* were not expressed, such as long-term hematopoietic stem cells (LT-HSC) and pre-pro-B cells (Fig. S3 C), consistent with a RAG-related function. We reasoned that if the reduced chromatin accessibility of the putative enhancer for the *Rag* locus was reflected in its activity in *Mki67*$^{-/-}$ pro-B and small pre-B cells, there would be an impact on expression of *Rag1* and/or *Rag2*. This possibility was assessed by RT-qPCR for both *Rag1* and *Rag2* and revealed that indeed *Rag1* mRNA expression in *Mki67*$^{-/-}$ pro-B and small pre-B cells was decreased approximately twofold in comparison with WT; the expression of *Rag2* was unaltered (Fig. 4 C). In contrast, the mRNA expression of the B cell lineage specification factor, *Pax5*, was not different between strains (Fig. S3 D), despite reduced accessibility at this gene locus in *Mki67*$^{-/-}$ B cell progenitors. Hence, Ki67 deficiency significantly alters chromatin accessibility at the *Rag* locus, and *Rag1* expression is selectively reduced in B cell progenitors.

Having determined reduced *Rag1* mRNA expression in Ki67-deficient B cell precursors, we assessed if there was an effect on Ig gene rearrangement. Ig gene rearrangement is tightly regulated during development with rearranged D_H to J_H at both *Igh* alleles in pro-B cells and V_H to DJ_H rearrangements leading to one productive *Igh* allele per cell in large pre-B cells (Fig. 4 D) (Mostoslavsky et al., 2004). We used qPCR to assess the loss of DNA that follows the joining of D_H to J_H segment clusters or of V_H to D_H elements. Pro-B and large pre-B cells were sorted from *Mki67*$^{-/-}$ and WT BM (as per Fig. 2), and genomic DNA was extracted. Sorted large pre-B cells were confirmed as such by expression of intracellular μ chain (Fig. S3, E and F), reflecting successful $V_HD_HJ_H$ rearrangement at one *Igh* allele and confirming the coordination of gene rearrangement and this B cell developmental stage. After normalizing for cell input, we determined that in *Mki67*$^{-/-}$ pro-B cells, the DNA between the D_H and J_H clusters was overrepresented compared with WT cells, meaning reduced D_HJ_H rearrangements compared with WT cells (Fig. 4 E). Similarly, *Mki67*$^{-/-}$ large pre-B cells retained a comparative excess of germline DNA positioned between the V_H and D_H segment clusters, indicative of an underrepresentation of $V_HD_HJ_H$ rearrangements (Fig. 4 F). We also noted a significant reduction in the relative frequencies of V(D)J rearrangement between all the J_H segments and the distal V_HJ558 (V_H1) cluster in *Mki67*$^{-/-}$ pre-B cells (Fig. S3 G), consistent with abnormalities in receptor gene rearrangement. While there may be pathways compensating for the loss of Ki67 in in vivo cell proliferation, possibly explaining why other hematopoietic lineages are unaffected, that no such compensation is possible in V(D)J rearrangement emphasizes the sensitivity of developing lymphocytes to abnormalities in this unique process. Collectively, these data demonstrate that Ki67 deficiency reduces V(D)J gene rearrangement during B cell development, and this is correlated with altered chromatin and reduced expression at the *Rag* locus.

Pre-rearranged Ig chains rescue *Mki67*-deficient B cell development

We reasoned that if impaired gene rearrangement contributed to impeding B cell development in the absence of Ki67, this would be reversed by pre-rearranged Ig chains. Accordingly, we separately crossed the *Mki67*$^{-/-}$ alleles onto the *Rag1*$^{-/-}$$SW_{HEL}$-$HC^{Ki/Ki}$ background, homozygous for pre-rearranged *Igh* alleles, and onto the *Rag1*$^{-/-}$$SW_{HEL}$-$HC^{Ki/Ki}LC^{Tg/+}$ background bearing pre-rearranged alleles at both *Igh* and *Igκ* loci (Phan et al., 2003). In *Mki67*-sufficient, *Rag1*-deficient mice, B cell development in

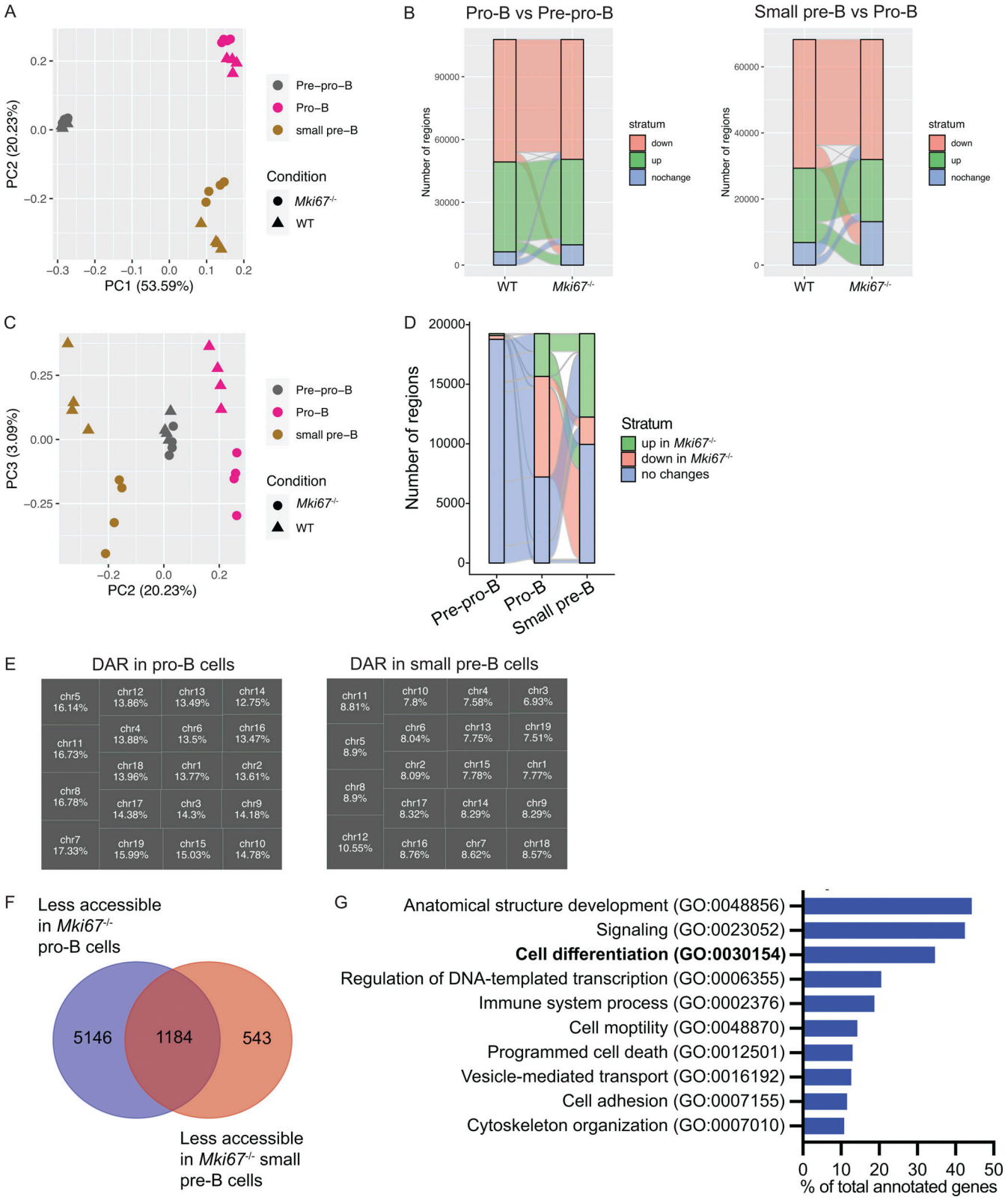

Figure 3. **Ki67 is required for maintaining global chromatin accessibility in B cell progenitors undergoing gene rearrangement. (A)** PCA of pre-pro-B, pro-B, and small pre-B cells from WT (n = 4) or *Mki67*$^{-/-}$ (n = 4) mice using all peaks showing PC1 versus PC2. **(B)** Sankey plots showing chromatin state across stage transitions from pre-pro-B to pro-B cells (left panel) and from pro-B to small pre-B cells in WT and *Mki67*$^{-/-}$ cells (right panel). **(C)** PCA of pre-pro-B, pro-B, and small pre-B cells from WT (n = 4) or *Mki67*$^{-/-}$ (n = 4) mice using all peaks showing PC2 versus PC3. **(D)** Sankey plot of numbers and status of all peaks in pre-pro-B, pro-B, and small pre-B cells comparing *Mki67*$^{-/-}$ to WT genotype. **(E)** Percentages of open chromatin regions altered in each chromosome in *Mki67*$^{-/-}$ pro-B and small pre-B cells in comparison to WT cells. **(F)** Venn diagrams of consistently less accessible regions in both *Mki67*$^{-/-}$ pro-B and small pre-B cells in comparison with WT cells. **(G)** Top 10 GO terms enriched in the genes annotated within the commonly less accessible regions in pro-B and small pre-B cells in the absence of Ki67. Data are from one experiment with four mice in WT or *Mki67*$^{-/-}$ group.

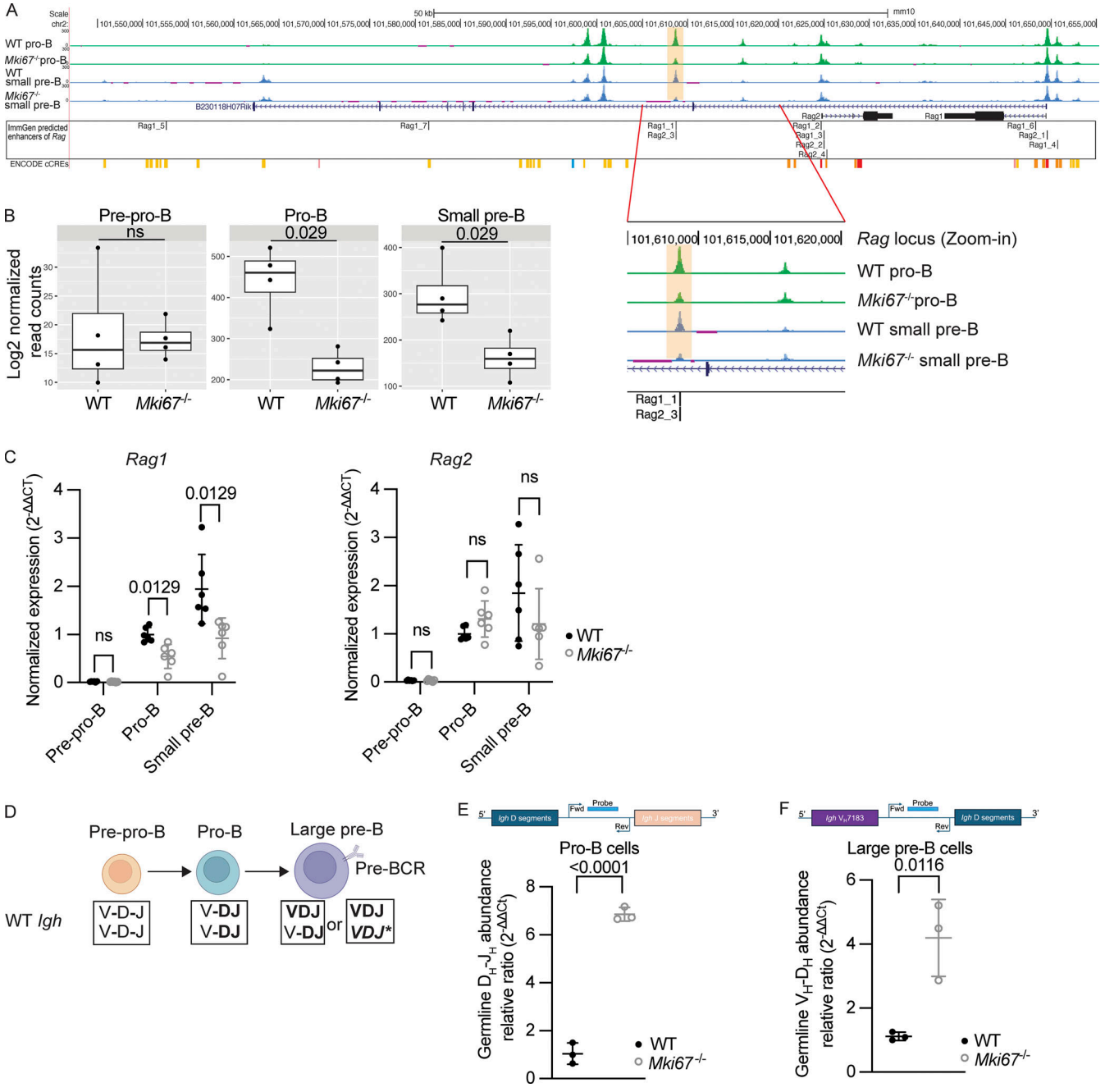

Figure 4. **Ki67 deficiency reduces accessibility at the *Rag* locus, decreases mRNA expression of *Rag1*, and impairs V(D)J gene rearrangement in B cell progenitors. (A)** Accessibility of the *Rag* locus (chr2:101,550,000–111,655,000) in the pro-B and small pre-B cells from WT and *Mki67*$^{-/-}$ mice. The putative enhancer region at the *Rag* locus annotated by ImmGen is highlighted. ENCODE candidate cis-regulatory elements (cCRE) are shown at the bottom. A zoomed-in image of the putative enhancer region at the *Rag* locus is shown. Data are representative of four mice from each group. **(B)** Quantification of the read counts of the putative enhancer region at the *Rag* locus in pre-pro-B, pro-B, and small pre-B cells from WT (n = 4) and *Mki67*$^{-/-}$ (n = 4) mice. Statistical differences were determined by Mann–Whitney tests with P values shown. ns, P > 0.05. **(C)** mRNA expression of *Rag1* and *Rag2* in pre-pro-B, pro-B, and small pre-B cells from WT (n = 6) and *Mki67*$^{-/-}$ (n = 6) mice by RT-qPCR. For each gene, CT values of each sample were first normalized by the CT values generated by a housekeeping assay (ΔCT) before being further normalized using one of the samples from the WT pro-B cells (ΔΔCT). All data points were finally normalized by fold-change against the mean of the $2^{-\Delta\Delta CT}$ values of the WT pro-B cells samples in each experiment. Data are merged from two independent experiments. Statistical differences were determined by multiple Mann–Whitney tests (corrected for multiple comparisons using the Holm–Sidak method) with adjusted P values shown. ns, P > 0.05. **(D)** Illustration of V(D)J rearrangement process of *Igh* locus in WT condition. V-D-J, *Igh* allele containing non-recombined germline V, D, and J gene segments; V-DJ, *Igh* allele containing non-recombined germline V gene segments; VDJ, successfully rearranged *Igh* allele; *VDJ**, non-productively rearranged *Igh* allele. **(E)** Relative abundance of germline sequences between D_H and J_H segments in WT (n = 3) or *Mki67*$^{-/-}$ (n = 3) pro-B cells measured by qPCR. CT values of each sample were first normalized by the CT values generated by a housekeeping assay (ΔCT) before being further normalized using one of the samples from the WT condition (ΔΔCT). **(F)** Relative abundance of germline sequences between V_H and D_H segments in WT (n = 3) or *Mki67*$^{-/-}$ (n = 3) large pre-B cells measured by qPCR. ΔΔCT was calculated as described in E. Schematic diagrams showing the positions of primers used for amplifying germline sequences are illustrated in E and F. Data in E and F are representative of two independent experiments. Statistical differences were determined in E and F by two-tailed unpaired t test with P values shown.

the presence of a pre-rearranged *Igh* allele comprised pre-pro-B and large and small pre-B, with the pro-B cell stage being absent (Fig. 5, A and B). When pre-rearranged *Igh* and *Igκ* alleles were both present, B cell development comprised pre-pro-B and immature B with pro-B and pre-B stages absent (Fig. 5, C and D). Importantly, in *Mki67*$^{-/-}$*Rag1*$^{-/-}$SW$_{HEL}$-HC$^{Ki/Ki}$ mice, the pre-rearranged H chain restored the number of large pre-B cells to that in *Mki67*-sufficient controls (Fig. 5, A and B), while small pre-B cell numbers recovered from a nine-fold deficit as seen in *Mki67*$^{-/-}$ mice without the pre-rearranged H chain (Fig. 2 E) to a three-fold deficit (Fig. 5, A and B), indicating a possible role for Ki67 in this compartment outside gene rearrangement. While this remains undefined, we noted an increase in apoptosis in small pre-B cells in the absence of Ki67 (Fig. S3, H and I), which is in line with the moderate increase of active Caspase-3 in *Mki67*$^{-/-}$ mouse tumors (Mrouj et al., 2021). The presence of pre-rearranged *Igh* and *Igκ* alleles fully reversed the deficit of immature B cells in BM of *Mki67*-deficient mice (Fig. 5, C and D). Interestingly, B cell representation was also equal in the spleens of *Mki67*-sufficient and -deficient *Rag1*$^{-/-}$SW$_{HEL}$-HC$^{Ki/Ki}$LC$^{Tg/+}$ mice (Fig. 5 E). Hence, our results identify a novel role for Ki67 in facilitating gene rearrangement at the antigen–receptor loci, thereby permitting normal B lymphocyte development.

Despite correctly configured lymphocytes being fundamental to immunity, our understanding of their development and the factors regulating it remains incomplete as exemplified by our finding Ki67 to be an important component. Using a novel, germline knockout mouse strain, we comprehensively characterized the lymphoid compartment in *Mki67*$^{-/-}$ mice, observing for what we believe is the first time that Ki67 is required for normal V(D)J rearrangement. While the requirement is not absolute in that both mature T and B cells are present in the periphery, the efficiency of development is impeded dramatically in both lineages. That B cell development in *Mki67*$^{-/-}$ mice is completely restored by the provision of pre-rearranged genes encoding H and L chains strongly indicates that the nature of the defect is gene rearrangement itself, which is further implicated by our finding of altered chromatin accessibility at the *Rag* locus and reduced mRNA expression of *Rag1*.

V(D)J rearrangement is a multistep process requiring chromatin remodeling for accessibility and large-scale changes in 3D genome architecture such as antigen receptor locus compartmentalization and contraction (Bossen et al., 2012; Johanson et al., 2019). Here, we show that Ki67 deficiency disrupts chromatin accessibility in B cell progenitors, especially at the stages representing developmental checkpoints associated with V(D)J rearrangement. Although chromatin accessibility to the antigen–receptor loci in the developing B cells is unaltered in the absence of Ki67, accessibility to regions corresponding to critical genes involved in lymphocyte differentiation is partially decreased in *Mki67*$^{-/-}$ pro-B and small pre-B cells, including at a putative enhancer for *Rag1/2*. This in turn is associated with disrupted mRNA expression of one of these essential factors, *Rag1*, and with impaired V(D)J rearrangement. Interestingly, partial RAG deficiency in humans results in impaired B cell development and restricted B cell receptor (BCR) repertoire (Csomos et al., 2022). This is in line with our data showing that decreased mRNA expression of *Rag1* in *Mki67*$^{-/-}$ pro-B and small pre-B cells is associated with both altered efficiency in the extent of gene rearrangement at the *Igh* locus and dysregulated usage of V_H segments in completed V(D)J rearrangements, indicative of an altered BCR repertoire in those cells. While our proposed mechanism is based on experimental evidence, a limitation is that it has not been formally demonstrated that a partial decrease of *Rag1* expression (approximately two-fold) as seen in *Mki67*$^{-/-}$ pro-B and small pre-B cells fully accounts for the defects in B cell development in *Mki67*$^{-/-}$ mice. Equally, it has yet to be proven that the same mechanism will explain the deficit in *Mki67*$^{-/-}$ thymocytes. It is also important to note that first, development itself largely was intact in *Mki67*$^{-/-}$ B cell precursors since all large pre-B cells were positive for intracellular Ig μ H chain, and second, there were few impediments to *Mki67*$^{-/-}$ B cell development outside of Ig gene rearrangement since it progressed to completion following provision of pre-rearranged H and L chains. However, it remains to be determined whether those *Mki67*$^{-/-}$ cells that successfully complete gene rearrangements then function normally in the periphery.

While changes in 3D genome architecture are required for gene rearrangement (Johanson et al., 2019), previous Hi-C data from Ki67-depleted cancer cell lines did not reveal detectable effects on 3D genome interactions (van Schaik et al., 2022). Of course, this does not exclude cell type–specific genome architectures being maintained by Ki67 but rather that any contribution of Ki67 in maintaining 3D genome organization in different cell types and/or in specific biological processes remains to be resolved. It is worth noting here our finding that a pre-rearranged *Igh* allele restored large but not small pre-B numbers in *Mki67*$^{-/-}$ mice. While we observed increased apoptosis in this exact cell stage of *Mki67*$^{-/-}$ B cells, which possibly accounts for the continued deficit, it indicates that there are non-rearrangement functions for Ki67. Curiously, this attribute was only apparent in small pre-B stage as a normal number of immature B cells was generated in the absence of Ki67 when both transgenic H and L chains were present. That is, this non-rearrangement activity of Ki67 is apparently quite limited in stage as well as in scale.

Taken together, our discovery of a distinct role for Ki67 in sustaining proper V(D)J rearrangement during lymphocyte development expands the knowledge of the physiological function of Ki67 and reinforces the importance of this fundamental biological process for a complete immune system.

Materials and methods

Animals

Mice were bred and maintained in specific pathogen–free facilities of the Monash University Animal Research Platform, Melbourne, Australia. *Mki67*$^{-/-}$, *Rag1*$^{-/-}$SW$_{HEL}$-HC$^{Ki/Ki}$, *Rag1*$^{-/-}$SW$_{HEL}$-HC$^{Ki/Ki}$LC$^{Tg/+}$, B6.SJL-^{Ptprca}/^{Ptprca} (CD45.1), and C57BL/J6 (CD45.2) mice were used in the study. Animal housing and all experiments were conducted in accordance with ethics protocols approved by the Alfred Research Alliance Animal Ethics Committee or Ozgene Animal Ethics Committee. Both female and male mice were used, sex- and age-matched across experiments.

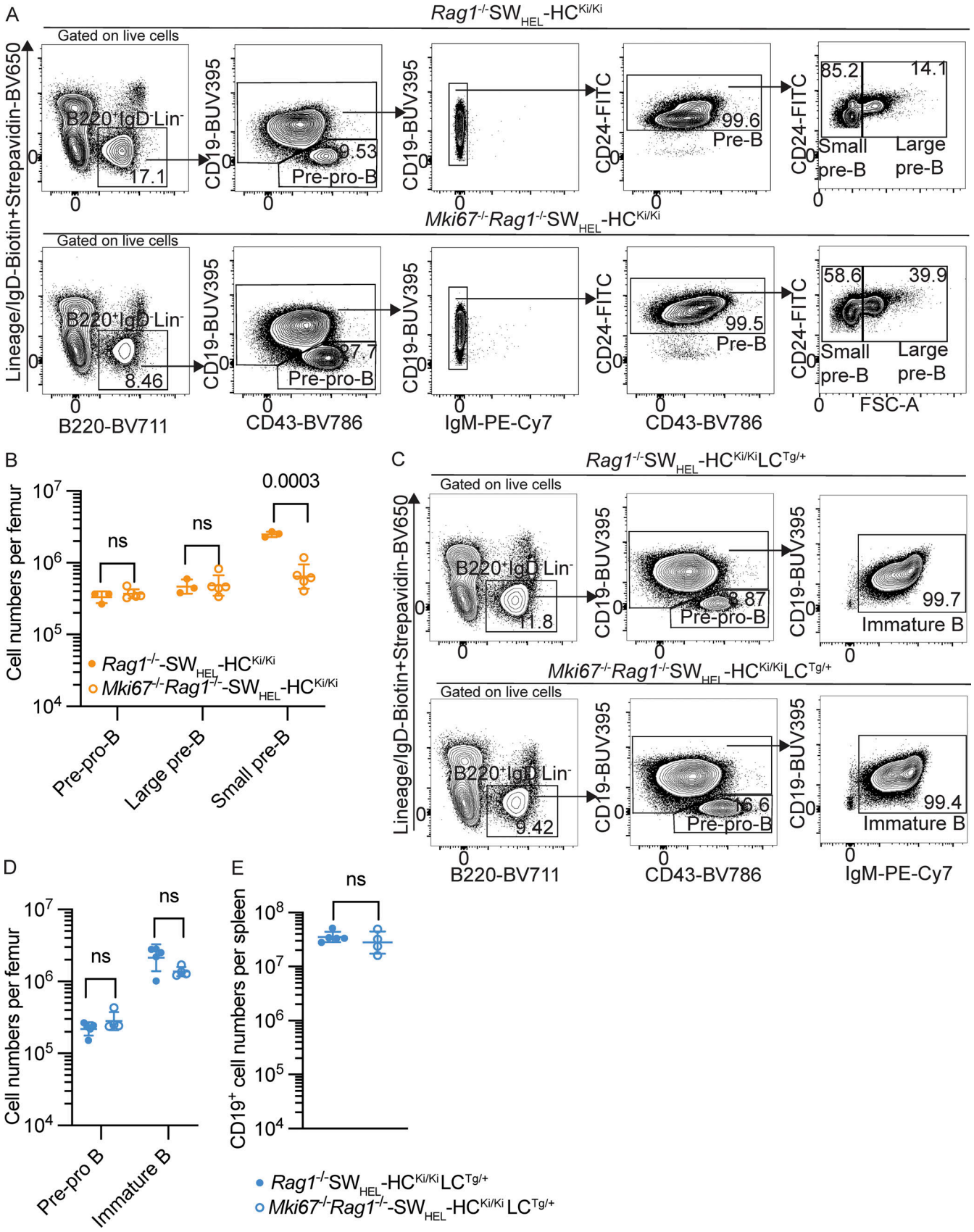

Figure 5. **Defects in early B cell development in *Mki67*$^{-/-}$ mice are rescued by pre-rearranged H and L chains. (A)** Gating strategy of pre-pro-B, large pre-B, and small pre-B cells when a pre-rearranged H chain was present in the WT- (*Rag1*$^{-/-}$SW$_{HEL}$-HC$^{Ki/Ki}$) or *Mki67*$^{-/-}$-*Rag1*–deficient (*Mki67*$^{-/-}$*Rag1*$^{-/-}$SW$_{HEL}$-HC$^{Ki/Ki}$) condition. Representative percentages of the gated populations of the parental gate are shown. **(B)** Quantification of cell numbers of pre-pro-B, large

pre-B, and small pre-B cells per femur in WT- (n = 3) or *Mki67*$^{-/-}$- (n = 5) *Rag1*$^{-/-}$SW$_{HEL}$-HC$^{Ki/Ki}$ mice. **(C)** Gating strategy of pre-pro-B and immature B cells when both pre-rearranged H and L chains were present in the WT- (*Rag1*$^{-/-}$SW$_{HEL}$-HC$^{Ki/Ki}$LC$^{Tg/+}$) or *Mki67*$^{-/-}$-*Rag1*$^{-/-}$ (*Mki67*$^{-/-}$*Rag1*$^{-/-}$SW$_{HEL}$-HC$^{Ki/Ki}$LC$^{Tg/+}$) conditions. Representative percentages of the gated populations of the parental gate are shown. **(D)** Quantification of cell numbers of pre-pro-B and immature B cells per femur in WT- (n = 5) or *Mki67*$^{-/-}$- (n = 4) *Rag1*$^{-/-}$SW$_{HEL}$-HC$^{Ki/Ki}$LC$^{Tg/+}$ mice. **(E)** Quantification of cell numbers of CD19$^+$ B cells per spleen in WT- (n = 5) or *Mki67*$^{-/-}$- (n = 4) *Rag1*$^{-/-}$SW$_{HEL}$-HC$^{Ki/Ki}$LC$^{Tg/+}$ mice. All data are representative of two independent experiments. Statistical differences were determined in B by multiple unpaired t tests (corrected for multiple comparisons using the Holm–Sidak method) and in D and E by two-tailed unpaired t test. P values or adjusted P values are shown. ns, P > 0.05.

Generation and characterization of the *Mki67*$^{-/-}$ strain

The targeted embryonic stem cells were microinjected into go-Germline (Koentgen et al., 2016) (Ozgene) blastocysts and transferred into pseudopregnant recipients. Each injection session consisted of transfers to two recipients, with each receiving ∼12 blasts in the transfer. The resultant offspring were assessed for chimerism. Male chimeras were crossed directly to a ubiquitous Cre strain (C57BL/6J-(ROSA)$^{26Sortm1(Ubic-CRE)Ozg/Ozg}$) at 6 wk of age. The crossing generated the first heterozygous knockout mice (*Mki67*$^{+/-}$), which were then intercrossed to produce the homozygous knockout line (*Mki67*$^{-/-}$). The H&E histology of the various tissues (Fig. S1 H) was performed and scored by Cerberus Sciences.

BM reconstitution

For BM reconstitution, recipient mice received 2 × 4.25 Gy doses of x-ray radiation 3 h apart and were then intravenously injected with 2 × 10^6 total BM cells from gender-matched donor mice. Mice received 1.622 mg/ml neomycin trisulfate salt hydrate (Sigma-Aldrich) in sterile water ad libitum for 2 wk after reconstitution.

Tissue preparation

Spleens and BM were dissected and processed as described (Robinson et al., 2023). Briefly, splenocyte suspensions were treated with red blood cell lysing buffer (156 mM NH_4Cl, 11.9 mM $NaHCO_3$, and 97 µM EDTA; pH = 7.3), washed in flow buffer (0.5% bovine serum albumin and 2 mM EDTA [Sigma-Aldrich] in PBS), and filtered through a 50-µm nylon mesh. BM cells were eluted from femurs by flushing with flow buffer and filtered through nylon mesh. BM samples were used without red blood cell lysis.

RT-qPCR for *Rag1*, *Rag2*, and *Pax5* mRNA

Cells were lysed and RNA extracted following the manufacturing instructions of the Qiagen RNeasy Plus Micro Kit. First-strand cDNA synthesis was performed as described (Robinson et al., 2019). cDNA samples were diluted as 1:2 with TE buffer (10 mM Tris and 0.1 mM EDTA) for use in qPCR. Reactions were set up per standard assay protocols from Integrated DNA Technologies (1× gene expression mastermix, probes at 250 nM, primers at 500 nM for both target and housekeeping assays) in a total volume of 20 µl, and cycling parameters were set as 95°C for 3 min followed by 45 cycles of 5 s at 95°C and 30 s at 62°C. Data were generated and analyzed by Thermo Fisher Scientific QuantStudio6 Real-Time PCR system utilizing the ΔΔCT (cycle threshold) method where ΔCT values were first calculated as $CT_{target} - CT_{Housekeeping}$ and then further normalized against CT values of one of the WT pro-B cells samples. All data points were finally normalized by fold change against the mean of the $2^{-\Delta\Delta C^T}$ values of the WT pro-B cells samples in each experiment. Probes and primers used were as below. The probe for the housekeeping gene was conjugated with Cy5 and probes for *Rag1* and *Rag2* were conjugated with fluorescein amidite (FAM) (all from Integrated DNA Technologies).

Housekeeping gene (Eef2)

Primer (reverse) 5′-GTCGCAGCTCTTAATACCCAT-3′
Primer (forward) 5′-GATCACCATCCACTTACCATCC-3′
Probe 5′-CCGTCACTGCACAGAAGTACCGTT-3′

Rag1

Primer (reverse) 5′-GAATTTCATCGGGTGCAGAA-3′
Primer (forward) 5′-AACCAAGCTGCAGACATTC-3′
Probe 5′-TTGCCGTCTACCCTGAGCTTCAG-3′

Rag2

Primer (reverse) 5′-ACAAGTTAGCAGGGCGTATATT-3′
Primer (forward) 5′-CTTCAGGATGGGCTGTCTTT-3′
Probe 5′-TTTGGGAGGACACTCACTTGCCA-3′

Pax5

Primer (reverse) 5′-ATTCGGCACTGGAGACTC-3′
Primer (forward) 5′-CTCATACTCCATCAGTGGCATC-3′
Probe 5′-ACACCAACAAACGCAAGAGGGATG-3′

qPCR for germline junction sequences between V_H, D_H, and J_H segments and recombined sequences between V_HJ588 and J_H1–4 segments

Cells were first lysed in 50 µl lysis buffer (1 mM EDTA, 10 mM Tris-HCl, pH 8.0, 40 mM NaCl, 0.1% SDS, and 90 µg/ml Proteinase K) at 56°C shaking at 225 rpm for 30 min and then heat-inactivated for 10 min at 95°C. Samples were diluted as 1:2 with TE buffer for use in qPCR. Reactions and cycling parameters were set up per standard assay protocols from Integrated DNA Technologies as described above. As a control, a sequence downstream from the *Igh* locus, not targeted by V(D)J recombination, was used as described (Braikia et al., 2014). Data were generated and analyzed by Thermo Fisher Scientific QuantStudio6 Real-Time PCR system utilizing the ΔΔCT method where ΔCT values were first calculated as $CT_{target} - CT_{Housekeeping}$ and then further normalized against CT values of one of the WT samples. The probes and primers used were as below. The probe for the housekeeping sequence was conjugated with hexachlorofluorescein, and the probes for target sequences were conjugated with FAM (all from Integrated DNA Technologies).

Germline junction sequences between D_H and J_H segments

Primer (reverse) 5′-GGGCCCATCCAGTTGAATTA-3′
Primer (forward) 5′-ACCAAACCCATCCCAAAGT-3′
Probe 5′-AGTGGCATCCAAGCCTCAGAAACT-3′

Germline junction sequences between V_H and D_H segments
Primer (reverse) 5′-AAATGAATGTGGTGATTGGCC-3′
Primer (forward) 5′-GGGGAGATCCATGAAGAGAAG-3′
Probe 5′-CGAGTAGGTGAGCTAGAGTAGCCT-3′

Recombined sequences between V_H588 and J_H1 segments
Primer (reverse) 5′-CCTGGGRCTTCAGTGAA-3′
Primer (forward) 5′-CAGAATGGAATGTGCAGAAAGA-3′
Probe 5′-AAAGCCAGCTTACCTGAGGAGACG-3′

Recombined sequences between V_H588 and J_H2 segments
Primer (reverse) 5′-CCTGGGRCTTCAGTGAA-3′
Primer (forward) 5′-GAAGAGAGAGGTTGTAAGACTC-3′
Probe 5′-ACCTGAGGAGACTGTGAGAGTGGT-3′

Recombined sequences between V_H588 and J_H3 segments
Primer (reverse) 5′-CCTGGGRCTTCAGTGAA-3′
Primer (forward) 5′-GAATGGGAGAAGTTAGGACTCA-3′
Probe 5′-CCTGCAGAGACAGTGACCAGAGTC-3′

Recombined sequences between V_HJ588 and J_H4 segments
Primer (reverse) 5′-CCTGGGRCTTCAGTGAA-3′
Primer (forward) 5′-AGACCTGGAGAGGCCATT-3′
Probe 5′-AGGAGACGGTGACTGAGGTTCC-3′

Housekeeping sequences
Primer (reverse) 5′-GGCTCCAAAGAATGCAAGAAC-3′
Primer (forward) 5′-TGACTAGGTTCGCAGGAGA-3′
Probe 5′-ACGGAGTCTCACCAGCACACAC-3′

Radioactive Southern blot hybridization

DNA samples were digested with XbaI overnight and separated on a 1% agarose gel. DNA was transferred onto 0.45-µm Biodyne B Nylon Membrane (Thermo Fisher Scientific) and hybridized with 40 ng p32-dATP labeled probe overnight at 42°C under stringent conditions (10% dextran sulfate, 50 mM Tris-HCl, pH 7.5, 1 M NaCl, 1% SDS, 50% formamide, 2% polyvinylpyrrolidone, 0.2 mg/ml sheared salmon sperm, 2% Ficoll, 1% trisodium phosphate dodecahydrate). Membranes were washed with low stringency wash solution at 42°C (0.1% saline sodium citrate and 0.1% SDS) followed by a high stringency wash (0.1% saline sodium citrate and 0.5% SDS) at 60°C. Membranes were exposed to an imaging screen-K (BioRad) for 48 h, and data were acquired with a Typhoon FLA (GE). Hybridization probes were generated as synthetic DNA gblocks (Integrated DNA Technologies) per the sequences below and radiolabeled with P32 using the Ambion DECAprime II kit (AM-1456, Applied Biosystems) and P32-dATP (Perkin Elmer).

5′ Probe:
5′-TCTCCTAAACTGACAGAAAGTTCTCTTTTATTTGTG
TCTTGTAATTATAACTACTTACATGAAAAGTAATTGTGTGTG
CTAGTATTTTCTAATATAATTATTCTGAAGTACTAGAAG
TCTCCATCTTTTATGGTTTCATAGGCAGTACTTGTGAACATT
GCCCTGCCCCTCATATCTTGTCAGTCCTTGTGTCGTTACACT
TATAATATAAACATACTAGTCAAATTCTGCTAATATTTTGAA
AACTTGAGGGTTTCTTTTTTTTTGTTGCATACCCTCATAAAT
CCCTT-3′.

3′ Probe:
5′-TCATCTACATTGTTTTGCATGGGGAATGAGATAATGTAA
GCCATGTTTCCAATGTTTTCCTTTATCAGGACTAACTGAAAT
GTTCAAGACTCCAGTGAAGGAGAAGCAGCAGCAGATGAGTGA
TACAGGCTCCGTACTTTCCAATTCAGCGAATTTGTCTGAAAG
ACAATTGCAAGTAACTAATTCAGGAGACATACCTGAGCCCAT
CACCACAGAGATTTTGGGTTGGTTTATTTGTCTTTTCCAATG
TTAAACTTTGGAATGGAGACTTGAAGACTGCCTTTTCTTTAT
AGACAATACTGGGTTCCTTCTCTACAATAGCTTTTCCTGGTG
AAATGCCGTTTCCACTTTCTCTGTTCTGTT-3′.

Western blot

Cells were lysed in 2× Laemmli buffer (Cat#1610737; BioRad Laboratories) and the proteins separated on an Any kD Mini-PROTEAN TGX precast protein gel (Cat#4569036; BioRad Laboratories). Samples were transferred onto a Trans-Blot Turbo RTA Mini Nitrocellulose membrane (Cat#1704270; BioRad Laboratories), blocked with Blotto (5% skim milk powder, 0.1% Tween-20 in PBS), and incubated at 4°C overnight with primary antibodies (Table S2). Membranes were washed with 0.1% Tween-20 in PBS (PBST) and incubated with secondary antibodies (Table S2) for 1 h at room temperature and washed again with PBST. Immobilon Forte Western HRP substrate (Cat#WBLUF0100; Merck Millipore) was added for visualization, and images were acquired using a ChemiDoc imaging system (BioRad Laboratories).

Flow cytometry and cell sorting

Cell samples were first incubated with purified anti-FcγRII/III (clone 2.4G2) antibody and normal rat sera in 5 ml polystyrene tubes before stained with fluorescently labeled antibodies and molecules (Table S3). In some experiments, cells were subsequently fixed and permeabilized for cytoplasmic staining with the Cytofix/Cytoperm reagents (BD Biosciences). Singlets were identified according to forward and side scatter properties. Live cells were identified by exclusion with Fixable Viability dye efluor780 (Life Technologies). The data were analyzed using FlowJo software (Treestar, Inc.). For cell sorting by flow cytometry, samples were stained using fluorescently labeled antibodies and molecules (Table S3) and 10,000–50,000 pre-pro-B, pro-B, large pre-B, or small pre-B were sorted.

In vitro B cell culture

B cells were purified with the B cell negative isolation kit (Cat#130-090-862; Miltenyi Biotec) and labeled with 5 µM Cell Trace Violet (CTV, Cat#C34557; Life Technologies Australia Pty Limited). Cells were incubated at 37°C in 5% CO_2 for 3.5 days in 200 µl/well B cell medium under anti-CD40 antibody and IL-4 stimulation (Robinson et al., 2020).

ATAC-seq library preparation, sequencing, and data analysis

Sorted pre-pro-B, pro-B, and small pre-B cells were pelleted, and a one-step permeabilization and tagmentation method was used as described (Di Pietro et al., 2022). Libraries were indexed and sequenced by a NovaSeq 6000 platform (Illumina). ATAC-seq data were processed with Nextflow pipeline (https://github.com/alexyfyf/atac_nf) (Yan et al., 2020). FASTQ files were quality-checked with FastQC (0.11.8) (Andrews, 2010) and

trimmed with trimmomatic (0.39) (Bolger et al., 2014) to remove low-quality reads and bases, and adapter sequences. Trimmed FASTQ files were aligned to mouse genome (mm10) with bwa-mem (0.7.17-r1188), and low-quality (<Q30), duplicated and unmapped reads were removed (Li and Durbin, 2009). Filtered BAM files were shifted to account for the 9-bp gap of Tn5 binding and peak calling was performed using MACS2 (2.2.7.1) with the following parameters: –q 0.01 --nomodel --shift –75 --extsize 150 --call-summits --keep-dup all (Zhang et al., 2008). BAM files were converted to bigwig files for visualization using deepTools (3.5.0) with reads per genomic content normalization (Ramirez et al., 2016). Consensus peak set was obtained by merging peaks in at least two samples and binding signal matrix was obtained by counting and normalizing reads in the consensus peaks. DARs were obtained under DESeq2 framework in DiffBind (2.12.0) (false discovery rate < 0.05) (Stark and Brown, 2011). PCA plots were performed using normalized read counts in 123,596 consensus peaks. GO enrichment analysis was performed using PANTHER (Thomas et al., 2022). Public ATAC-seq data for LT-HSC and DN3 thymocytes and the annotations of putative enhancers at the *Rag* locus were obtained from the ImmGen database (Heng et al., 2008).

Statistical analysis and data visualization

Flow cytometry plots were generated with FlowJo software, data were exported into Excel (Microsoft) and then into Prism (GraphPad Software) for graphing and statistical analysis. Inset numbers in flow plots are percent of the parent gate. $P < 0.05$ was considered significant throughout. Data on linear axes are shown as mean + standard deviation (SD), and data on log axes are shown as geometric mean with error bars indicating the geometric SD factor. Statistical tests applied are stated in figure legends. Figures were compiled using Adobe Illustrator.

Online supplemental material

Fig. S1 shows the generation and validation of *Mki67*$^{-/-}$ mice. Fig. S2 characterizes the defects in early B and T cell development in the absence of Ki67. Fig. S3 shows chromatin accessibility at the *Igh* and *Igκ* loci in WT and *Mki67*$^{-/-}$ pro-B and small pre-B cells, chromatin accessibility at the *Rag* locus in LT-HSC, DN3, and WT and *Mki67*$^{-/-}$ pre-pro-B cells from either ImmGen database or our own data. Fig. S3 also shows the mRNA expression of *Pax5*, an abundance of rearranged V_HJ558 with all J_H segments, intracellular μ chain expression, and apoptosis in WT and *Mki67*$^{-/-}$ B cell progenitors. Table S1 shows annotated genes enriched in the GO term cell differentiation GO: 0030154. Table S2 shows antibodies used in western blot and flow cytometry. Table S3 shows the antibody panel used in flow cytometry.

Data availability

Raw ATAC-seq data underlying Figs. 3 and 4 are available on Gene Expression Omnibus with accession number GSE246986. All data are available in the article itself and its supplementary materials and are also available upon request from the corresponding authors.

Acknowledgments

We thank the Mouse Intensive Care Unit animal facility at Alfred Research Alliance and Monash Animal Research Platform for animal welfare, husbandry, and housing assistance, the Central Clinical School Genomic Facility for sequencing assistance, the Alfred Research Alliance FlowCore for cell sorting, and the Curtin Health Innovation Research Institute Flow Cytometry Core Facility for technical assistance.

This work was supported by the MASSIVE high performance computing facility (https://www.massive.org.au) and the Nectar research cloud for computing infrastructure. Z. Ding was supported by the Swedish Research Council International Postdoc Grant (2016-06659) and a Future Leader Postdoctoral Fellowship from Monash University. D.M. Tarlinton was funded by an Investigator Grant (APP1175411) awarded by the National Health and Medical Research Council (NHMRC) Australia and F. Yan by a Cancer Council Victoria Postdoctoral Research Fellowship. I. Quast was supported by an Advanced Postdoc Mobility Fellowship (P300PA_177893) provided by the Swiss National Science Foundation and a Peter Doherty Early Career Fellowship (APP1145136) provided by NHMRC Australia. This work was supported by NHMRC grants awarded to D.M. Tarlinton and I. Quast (APP1146617), M.J. Robinson and I. Quast (APP1185294), and M.J. Robinson and Z. Ding (APP2028727).

Author contributions: Z. Ding: Conceptualization, Data curation, Formal analysis, Investigation, Methodology, Project administration, Supervision, Validation, Visualization, Writing—original draft, Writing—review & editing, M. Hagan: Conceptualization, Investigation, Methodology, Resources, Writing—review & editing, F. Yan: Data curation, Formal analysis, Methodology, Resources, Software, Visualization, Writing—review & editing, N.W.Y. Schroer: Formal analysis, Investigation, Validation, Visualization, J. Polmear: Investigation, Writing—review & editing, K.L. Good-Jacobson: Methodology, Supervision, Writing—review & editing, A.R. Dvorscek: Investigation, Writing—review & editing, C. Pitt: Investigation, Methodology, K. O'Donnell: Investigation, S.L. Nutt: Supervision, Writing—review & editing, D. Zotos: Conceptualization, Data curation, Formal analysis, Methodology, Resources, Visualization, Writing—review & editing, C. McKenzie: Writing—review & editing, D.L. Hill: Formal analysis, Supervision, Writing—review & editing, M.J. Robinson: Funding acquisition, Investigation, Writing—review & editing, I. Quast: Conceptualization, Methodology, Writing—review & editing, F. Koentgen: Conceptualization, Funding acquisition, Methodology, Project administration, Resources, Supervision, Writing—review & editing, D.M. Tarlinton: Conceptualization, Formal analysis, Funding acquisition, Methodology, Project administration, Resources, Supervision, Visualization, Writing—original draft, Writing—review & editing.

Disclosures: The authors declare no competing interests exist.

Submitted: 22 November 2023
Revised: 10 April 2024
Accepted: 17 May 2024

References

Andrews, S. 2010. FastQC: a quality control tool for high throughput sequence data.. http://www.bioinformatics.babraham.ac.uk/projects/fastqc

Bolger, A.M., M. Lohse, and U. Usadle. 2014. *Bioinformatics*. 30:2114–2120. https://doi.org/10.1093/bioinformatics/btu170

Bossen, C., R. Mansson, and C. Murre. 2012. Chromatin topology and the regulation of antigen receptor assembly. *Annu. Rev. Immunol.* 30:337–356. https://doi.org/10.1146/annurev-immunol-020711-075003

Boya, R., A.D. Yadavalli, S. Nikhat, S. Kurukuti, D. Palakodeti, and J.M.R. Pongubala. 2017. Developmentally regulated higher-order chromatin interactions orchestrate B cell fate commitment. *Nucleic Acids Res.* 45: 11070–11087. https://doi.org/10.1093/nar/gkx722

Braikia, F.Z., G. Chemin, M. Moutahir, and A.A. Khamlichi. 2014. Quantification of V(D)J recombination by real-time quantitative PCR. *Immunol. Lett.* 162:119–123. https://doi.org/10.1016/j.imlet.2014.08.002

Cherry, S.R., and D. Baltimore. 1999. Chromatin remodeling directly activates V(D)J recombination. *Proc. Natl. Acad. Sci. USA*. 96:10788–10793. https://doi.org/10.1073/pnas.96.19.10788

Csomos, K., B. Ujhazi, P. Blazso, J.L. Herrera, C.M. Tipton, T. Kawai, S. Gordon, M. Ellison, K. Wu, M. Stowell, et al. 2022. Partial RAG deficiency in humans induces dysregulated peripheral lymphocyte development and humoral tolerance defect with accumulation of T-bet$^+$ B cells. *Nat. Immunol.* 23:1256–1272. https://doi.org/10.1038/s41590-022-01271-6

Cuylen, S., C. Blaukopf, A.Z. Politi, T. Müller-Reichert, B. Neumann, I. Poser, J. Ellenberg, A.A. Hyman, and D.W. Gerlich. 2016. Ki-67 acts as a biological surfactant to disperse mitotic chromosomes. *Nature*. 535: 308–312. https://doi.org/10.1038/nature18610

Cuylen-Haering, S., M. Petrovic, A. Hernandez-Armendariz, M.W.G. Schneider, M. Samwer, C. Blaukopf, L.J. Holt, and D.W. Gerlich. 2020. Chromosome clustering by Ki-67 excludes cytoplasm during nuclear assembly. *Nature*. 587:285–290. https://doi.org/10.1038/s41586-020-2672-3

Di Pietro, A., J. Polmear, L. Cooper, T. Damelang, T. Hussain, L. Hailes, K. O'Donnell, V. Udupa, T. Mi, S. Preston, et al. 2022. Targeting BMI-1 in B cells restores effective humoral immune responses and controls chronic viral infection. *Nat. Immunol.* 23:86–98. https://doi.org/10.1038/s41590-021-01077-y

Garwain, O., X. Sun, D.R. Iyer, R. Li, L.J. Zhu, and P.D. Kaufman. 2021. The chromatin-binding domain of Ki-67 together with p53 protects human chromosomes from mitotic damage. *Proc. Natl. Acad. Sci. USA*. 118: e2021998118. https://doi.org/10.1073/pnas.2021998118

Gerdes, J., U. Schwab, H. Lemke, and H. Stein. 1983. Production of a mouse monoclonal antibody reactive with a human nuclear antigen associated with cell proliferation. *Int. J. Cancer*. 31:13–20. https://doi.org/10.1002/ijc.2910310104

Germain, R.N. 2002. T-cell development and the CD4-CD8 lineage decision. *Nat. Rev. Immunol.* 2:309–322. https://doi.org/10.1038/nri798

Hardy, R.R., and K. Hayakawa. 2001. B cell development pathways. *Annu. Rev. Immunol.* 19:595–621. https://doi.org/10.1146/annurev.immunol.19.1.595

Heng, T.S., M.W. Painter, K. Elpek, V. Lukacs-Kornek, N. Mauermann, S.J. Turley, D. Koller, F.S. Kim, A.J. Wagers, N. Asinovski, et al. 2008. The immunological genome Project: Networks of gene expression in immune cells. *Nat. Immunol.* 9:1091–1094. https://doi.org/10.1038/ni1008-1091

Johanson, T.M., W.F. Chan, C.R. Keenan, and R.S. Allan. 2019. Genome organization in immune cells: Unique challenges. *Nat. Rev. Immunol.* 19: 448–456. https://doi.org/10.1038/s41577-019-0155-2

Koentgen, F., J. Lin, M. Katidou, I. Chang, M. Khan, J. Watts, and P. Mombaerts. 2016. Exclusive transmission of the embryonic stem cell-derived genome through the mouse germline. *Genesis*. 54:326–333. https://doi.org/10.1002/dvg.22938

Li, H., and R. Durbin. 2009. Fast and accurate short read alignment with Burrows-Wheeler transform. *Bioinformatics*. 25:1754–1760. https://doi.org/10.1093/bioinformatics/btp324

Lion, M., B. Muhire, Y. Namiki, M.Y. Tolstorukov, and M.A. Oettinger. 2020. Alterations in chromatin at antigen receptor loci define lineage progression during B lymphopoiesis. *Proc. Natl. Acad. Sci. USA*. 117: 5453–5462. https://doi.org/10.1073/pnas.1914923117

MacCallum, D.E., and P.A. Hall. 2000. The biochemical characterization of the DNA binding activity of pKi67. *J. Pathol.* 191:286–298. https://doi.org/10.1002/1096-9896(2000)9999:9999<::AID-PATH628>3.0.CO;2-J

Mandal, M., S.E. Powers, K. Ochiai, K. Georgopoulos, B.L. Kee, H. Singh, and M.R. Clark. 2009. Ras orchestrates exit from the cell cycle and light-chain recombination during early B cell development. *Nat. Immunol.* 10: 1110–1117. https://doi.org/10.1038/ni.1785

Melchers, F. 2015. Checkpoints that control B cell development. *J. Clin. Invest.* 125:2203–2210. https://doi.org/10.1172/JCI78083

Miller, I., M. Min, C. Yang, C. Tian, S. Gookin, D. Carter, and S.L. Spencer. 2018. Ki67 is a graded rather than a binary marker of proliferation versus quiescence. *Cell Rep.* 24:1105–1112.e5. https://doi.org/10.1016/j.celrep.2018.06.110

Mostoslavsky, R., F.W. Alt, and K. Rajewsky. 2004. The lingering enigma of the allelic exclusion mechanism. *Cell*. 118:539–544. https://doi.org/10.1016/j.cell.2004.08.023

Mrouj, K., N. Andres-Sanchez, G. Dubra, P. Singh, M. Sobecki, D. Chahar, E. Al Ghoul, A.B. Aznar, S. Prieto, N. Pirot, et al. 2021. Ki-67 regulates global gene expression and promotes sequential stages of carcinogenesis. *Proc. Natl. Acad. Sci. USA*. 118:e2026507118. https://doi.org/10.1073/pnas.2026507118

Ng, A.P., H.D. Coughlan, S. Hediyeh-Zadeh, K. Behrens, T.M. Johanson, M.S.Y. Low, C.C. Bell, O. Gilan, Y.C. Chan, A.J. Kueh, et al. 2020. An Erg-driven transcriptional program controls B cell lymphopoiesis. *Nat. Commun.* 11:3013. https://doi.org/10.1038/s41467-020-16828-y

Nutt, S.L., P. Urbánek, A. Rolink, and M. Busslinger. 1997. Essential functions of Pax5 (BSAP) in pro-B cell development: Difference between fetal and adult B lymphopoiesis and reduced V-to-DJ recombination at the IgH locus. *Genes Dev.* 11:476–491. https://doi.org/10.1101/gad.11.4.476

Phan, T.G., M. Amesbury, S. Gardam, J. Crosbie, J. Hasbold, P.D. Hodgkin, A. Basten, and R. Brink. 2003. B cell receptor-independent stimuli trigger immunoglobulin (Ig) class switch recombination and production of IgG autoantibodies by anergic self-reactive B cells. *J. Exp. Med.* 197:845–860. https://doi.org/10.1084/jem.20022144

Robinson, M.J., Z. Ding, M.R. Dowling, D.L. Hill, R.H. Webster, C. McKenzie, C. Pitt, K. O'Donnell, J. Mulder, E. Brodie, et al. 2023. Intrinsically determined turnover underlies broad heterogeneity in plasma-cell lifespan. *Immunity*. 56:1596–1612.e4. https://doi.org/10.1016/j.immuni.2023.04.015

Robinson, M.J., Z. Ding, C. Pitt, E.J. Brodie, I. Quast, D.M. Tarlinton, and D. Zotos. 2020. The amount of BCL6 in B cells shortly after antigen engagement determines their tepresentation in subsequent germinal centers. *Cell Rep.* 30:1530–1541.e4. https://doi.org/10.1016/j.celrep.2020.01.009

Ramirez, F., D.P. Ryan, V. Gruning, V. Bhardwaj, F. Kilpert, A.S. Richter, S. Heyne, F. Dunder, and T. Manke. 2016. deepTools2: a next generation web server for deep-sequencing data analysis. *Nucleic Acids Res.* 44: W160-165. https://doi.org/10.1093/nar/gkw257

Robinson, M.J., C. Pitt, E.J. Brodie, A.M. Valk, K. O'Donnell, L. Nitschke, S. Jones, and D.M. Tarlinton. 2019. BAFF, IL-4 and IL-21 separably program germinal center-like phenotype acquisition, BCL6 expression, proliferation and survival of CD40L-activated B cells in vitro. *Immunol. Cell Biol.* 97:826–839. https://doi.org/10.1111/imcb.12283

Scholzen, T., E. Endl, C. Wohlenberg, S. van der Sar, I.G. Cowell, J. Gerdes, and P.B. Singh. 2002. The Ki-67 protein interacts with members of the heterochromatin protein 1 (HP1) family: A potential role in the regulation of higher-order chromatin structure. *J. Pathol.* 196:135–144. https://doi.org/10.1002/path.1016

Sobecki, M., K. Mrouj, A. Camasses, N. Parisis, E. Nicolas, D. Llères, F. Gerbe, S. Prieto, L. Krasinska, A. David, et al. 2016. The cell proliferation antigen Ki-67 organises heterochromatin. *Elife*. 5:e13722. https://doi.org/10.7554/eLife.13722

Sobecki, M., K. Mrouj, J. Colinge, F. Gerbe, P. Jay, L. Krasinska, V. Dulic, and D. Fisher. 2017. Cell-cycle regulation accounts for variability in Ki-67 expression levels. *Cancer Res.* 77:2722–2734. https://doi.org/10.1158/0008-5472.CAN-16-0707

Stanhope-Baker, P., K.M. Hudson, A.L. Shaffer, A. Constantinescu, and M.S. Schlissel. 1996. Cell type-specific chromatin structure determines the targeting of V(D)J recombinase activity in vitro. *Cell*. 85:887–897. https://doi.org/10.1016/S0092-8674(00)81272-6

Stark, R., and G.D. Brown. 2011. DiffBind: Differential Binding Analysis of ChIP-Seq Peak Data. Bioconductor.. http://bioconductor.org/packages/release/bioc/html/DiffBind.html

Thomas, P.D., D. Ebert, A. Muruganujan, T. Mushayahama, L.P. Albou, and H. Mi. 2022. PANTHER: Making genome-scale phylogenetics accessible to all. *Protein Sci.* 31:8–22. https://doi.org/10.1002/pro.4218

van Schaik, T., S.G. Manzo, A.E. Vouzas, N.Q. Liu, H. Teunissen, E. de Wit, D.M. Gilbert, and B. van Steensel. 2022. Dynamic chromosomal interactions and control of heterochromatin positioning by Ki-67. *EMBO Rep.* 23:e55782. https://doi.org/10.15252/embr.202255782

von Freeden-Jeffry, U., N. Solvason, M. Howard, and R. Murray. 1997. The earliest T lineage-committed cells depend on IL-7 for Bcl-2 expression and normal cell cycle progression. *Immunity*. 7:147–154. https://doi.org/10.1016/S1074-7613(00)80517-8

Yan, F., D.R. Powell, D.J. Curtis, and N.C. Wong. 2020. From reads to insight: a hitchhiker's guide to ATAC-seq data analysis. *Genome Biol.* 21:22. https://doi.org/10.1186/s13059-020-1929-3

Yoshida, H., C.A. Lareau, R.N. Ramirez, S.A. Rose, B. Maier, A. Wroblewska, F. Desland, A. Chudnovskiy, A. Mortha, C. Dominguez, et al. 2019. The cis-regulatory atlas of the mouse immune system. *Cell*. 176:897–912.e20. https://doi.org/10.1016/j.cell.2018.12.036

Zhang, Y., T. Liu, C.A. Meyer, J. Eeckhoute, D.S. Johnson, B.E. Bernstein, C. Nusbaum, R.M. Myers, M. Brown, W. Li, et al. 2008. Model-based analysis of ChIP-Seq (MACS). *Genome Biol.* 9:R137. https://doi.org/10.1186/gb-2008-9-9-r137

JEM

Supplemental material

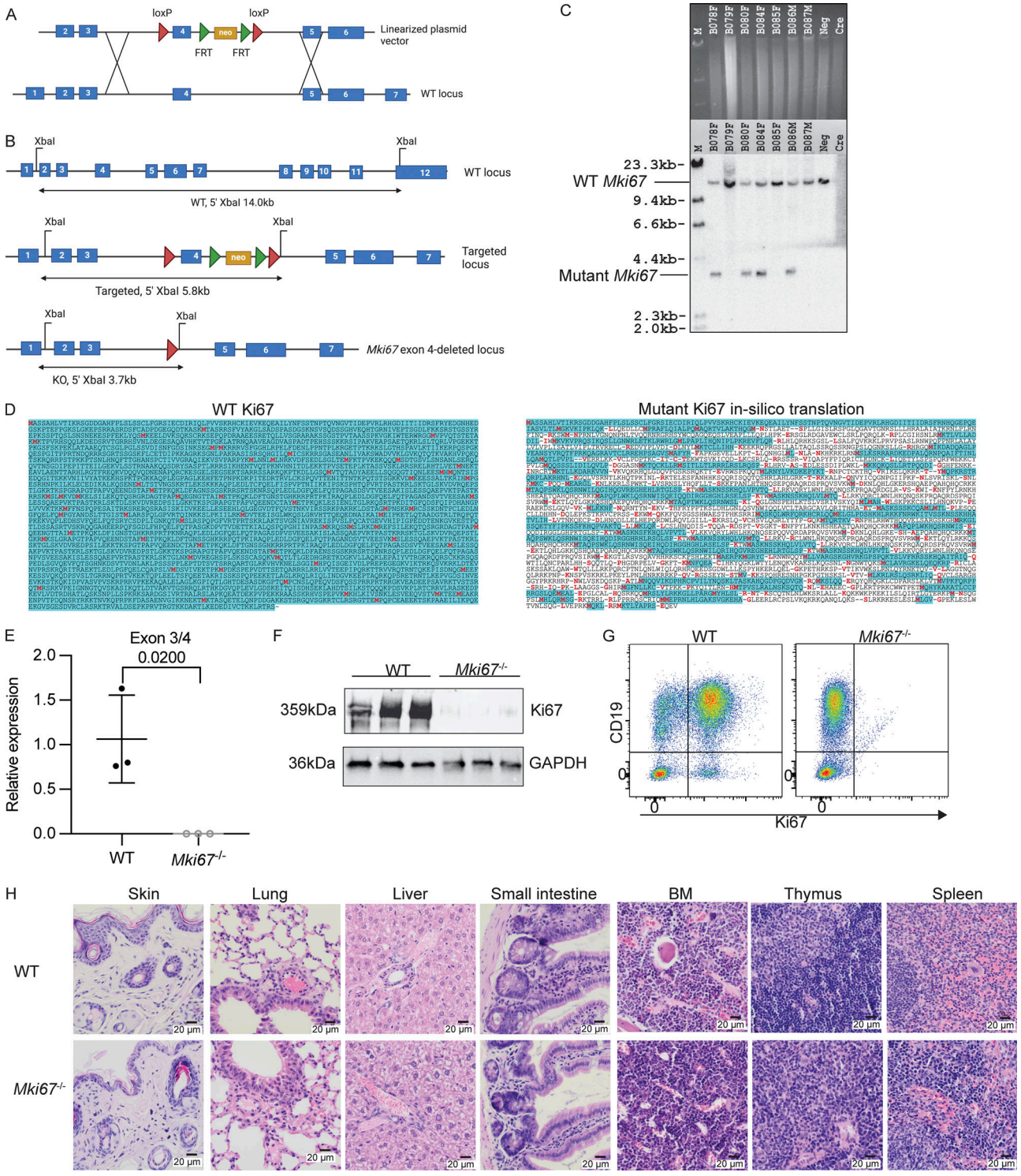

Figure S1. **Related to Fig. 1: The generation and validation of *Mki67*$^{-/-}$ mice deficient for Ki67. (A)** Schematic of the recombining strategy to target the *Mki67* locus. FRT, flippase recognition target. **(B)** Schematics of the Southern screening strategy used for genotyping embryonic stem cells and mice exhibiting XbaI restriction sites and expected band sizes from a 5′ hybridizing probe on WT, targeted, and knockout alleles. **(C)** Southern screens generated from mouse tissue biopsy samples showing WT *Mki67* bands at 14.0 kb and exon 4–deleted *Mki67* bands at 3.7 kb. **(D)** In silico translation by ExPASy of mutant Ki67 protein sequence in comparison to WT Ki67 protein sequence. Red, initiating amino acid; blue, where open reading frame is read; -, where stop codon is read. **(E)** RT-qPCR analysis of the relative abundance of the sequences across the exon 3–4 junction in the *Mki67* loci in liver samples from WT (n = 3) and *Mki67*$^{-/-}$ mice (n = 3). **(F)** Western blot analysis of Ki67 protein expression in WT (n = 3) and *Mki67*$^{-/-}$ (n = 3) splenocytes stimulated with 20 ng/ml LPS for 48 h. The expression of GAPDH was used as control. **(G)** Flow cytometry plot showing Ki67 protein expression in WT and *Mki67*$^{-/-}$ splenocytes stimulated with 20 ng/ml LPS for 48 h. Data are representative of three mice from each group. **(H)** Histology showing H&E staining of skin, lung, liver, small intestine, BM, thymus, and spleen sections from WT and *Mki67*$^{-/-}$ mice. Scale bars represent 20 μm. Data are representative of three mice from each group. Statistical significance between conditions in E was assessed by two-tailed unpaired t test with P value shown. Source data are available for this figure: SourceData FS1.

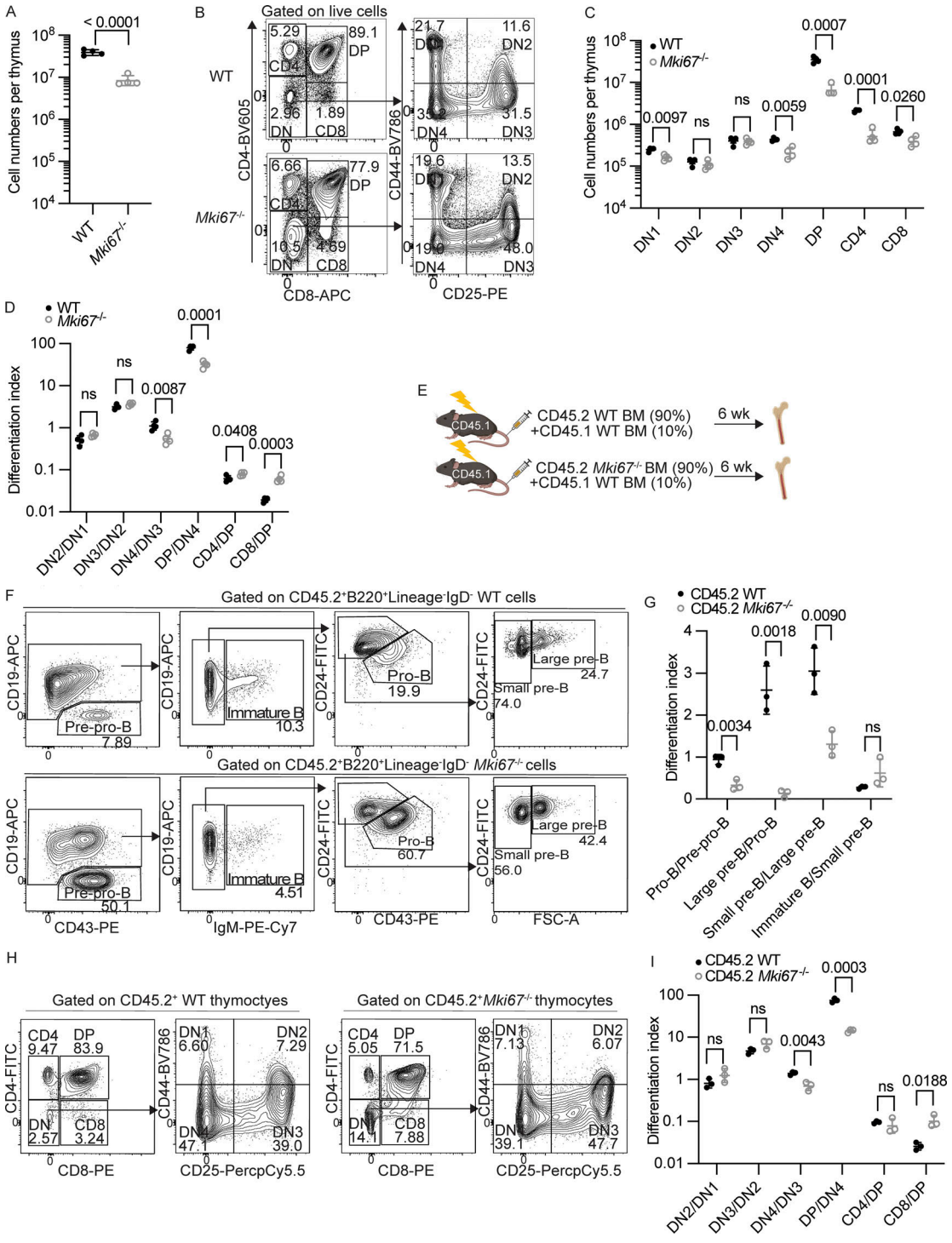

Figure S2. **Related to Fig. 2: Characterization of the defects in early B and T cell development in the absence of Ki67. (A)** Total cell counts of thymocytes in WT (n = 4) and *Mki67*$^{-/-}$ (n = 4) mice. **(B)** Gating strategy of T cell progenitors at DN1, DN2, DN3, DN4, DP, CD4, and CD8 in the thymus. Representative percentages of the gated populations of the parental gate are shown. **(C)** Quantification of cell numbers of DN1, DN2, DN3, DN4, DP, CD4, and CD8 per thymus in WT (n = 4) and *Mki67*$^{-/-}$ (n = 4) mice. **(D)** Differentiation indexes calculated as cell numbers of a later T cell developmental stage divided by that of the former stage in WT (n = 4) and *Mki67*$^{-/-}$ (n = 4) mice. **(E)** Schematic of the BM reconstitution setup. **(F)** Representative gating strategy for each stage among the CD45.2 B220^{+}IgD^{-}Lin^{-} B-lineage cells derived from the CD45.2 WT donor (n = 3) or *Mki67*$^{-/-}$ donor BM (n = 3). **(G)** Differentiation indexes calculated as cell numbers of a later B cell developmental stage divided by that of the former stage of B cell progenitors derived from the CD45.2 WT donor (n = 3) or *Mki67*$^{-/-}$ donor BM (n = 3). **(H)** Representative gating strategy for T cell progenitors at each stage among the CD45.2 thymocytes derived from the CD45.2 WT donor (n = 3) or *Mki67*$^{-/-}$ donor BM (n = 3). **(I)** Differentiation indexes calculated as cell numbers of a later T cell developmental stage divided by that of the former stage of T cell progenitors derived from the CD45.2 WT donor (n = 3) or *Mki67*$^{-/-}$ donor BM (n = 3). Data in A–D are representative of four independent experiments and in E–I two independent experiments. Statistical significances in A were determined by two-tailed unpaired t test and in C, D, G, and I by multiple unpaired t tests (corrected for multiple comparisons using the Holm–Sidak method). P values or adjusted P values are shown. ns, P > 0.05.

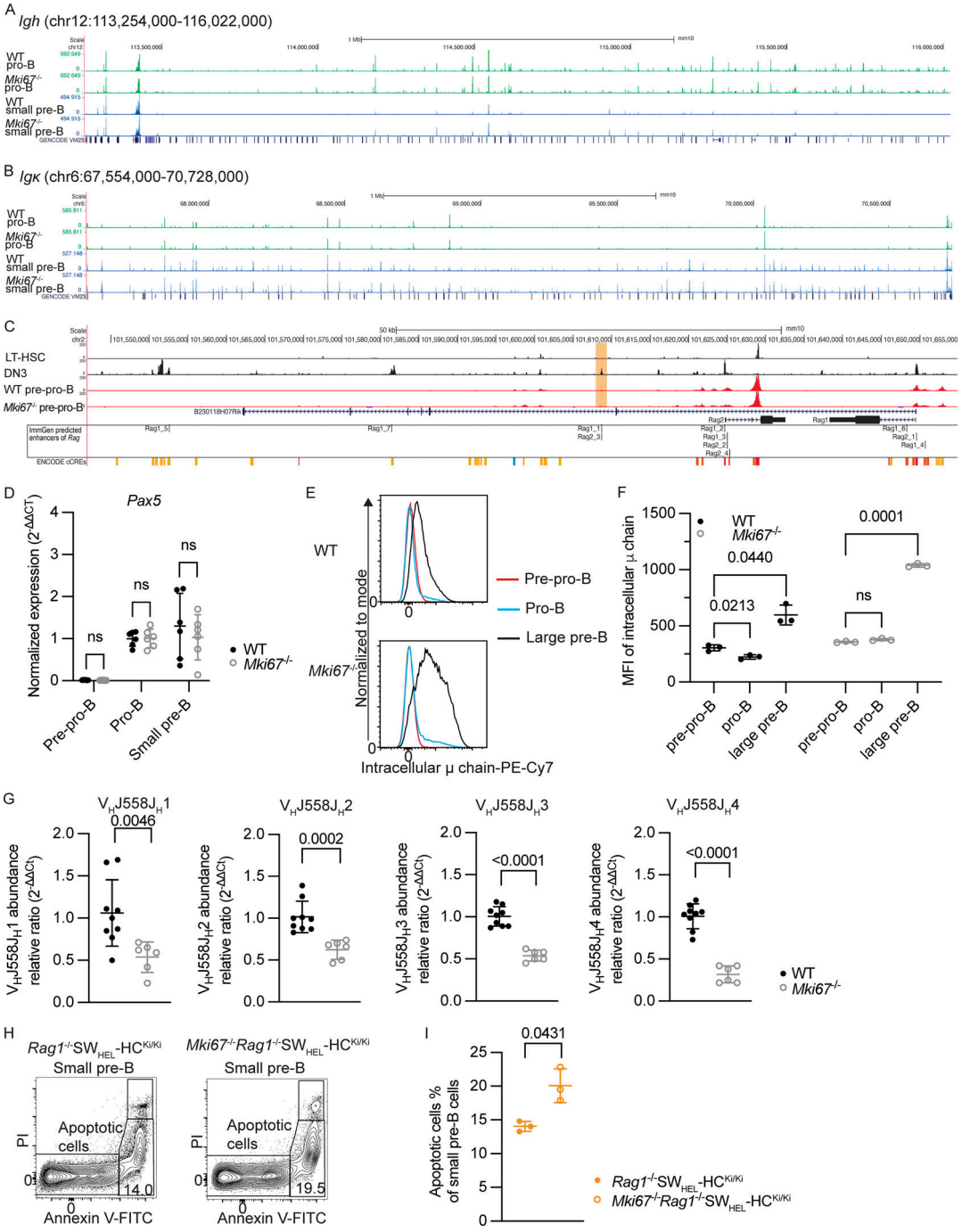

Figure S3. **Related to** Figs. 3, 4, and 5**: Chromatin accessibility, gene expression, VDJ_H rearrangement, and apoptosis in WT and *Mki67*$^{-/-}$ B cell progenitors. (A)** Accessibility of the *Igh* locus (chr12:113,254,000-116,022,000) in the pro-B and small pre-B cells from WT and *Mki67*$^{-/-}$ mice. Data are representative of four mice from each group. **(B)** Accessibility at the *Igκ* locus (chr6:67,554,000-70,728,000) in the pro-B and small pre-B cells from WT and *Mki67*$^{-/-}$ mice. Data are representative of four mice from each group. **(C)** Accessibility at the *Rag* locus (chr2:101,550,000–111,655,000) in LT-HSC and DN3 thymocytes from WT mice (obtained from the ImmGen database) and in pre-pro-B cells from WT and *Mki67*$^{-/-}$ mice (representative of four mice from each group). The putative enhancer region annotated by ImmGen database for the *Rag* locus is highlighted. **(D)** mRNA expression of *Pax5* in pre-pro-B, pro-B, and small pre-B cells from WT (n = 6) and *Mki67*$^{-/-}$ (n = 6) mice by RT-qPCR. Normalization was performed as described in Fig. 4. Data are merged from two independent experiments. Statistical differences were determined by multiple Mann–Whitney tests (corrected for multiple comparisons using the Holm–Sidak method). ns, P > 0.05. **(E)** Representative histograms showing intracellular μ chain expression in WT and *Mki67*$^{-/-}$ pre-pro-B, pro-B, and large pre-B cells. **(F)** Comparison of the median fluorescent intensity (MFI) of intracellular μ chain expression in WT (n = 3) and *Mki67*$^{-/-}$ (n = 3) pre-pro-B, pro-B, and large pre-B cells. Statistical differences were determined by one-way ANOVA using Dunnett's multiple comparisons tests. **(G)** The relative abundance of recombined V_HJ558 family members and each of the J_H1–4 segments in WT (n = 9) or *Mki67*$^{-/-}$ (n = 6) pre-B cells measured by qPCR. ΔΔCT was calculated as described in Fig. 4 E. Statistical differences were determined by two-tailed unpaired t test with P values shown. **(H)** Gating strategy of apoptotic cells among small pre-B cells from WT- or *Mki67*$^{-/-}$*Rag1*$^{-/-}$$SW_{HEL}$-$HC^{Ki/Ki}$ mice. **(I)** Quantification of percentages of apoptotic cells among the small pre-B cells from WT- (n = 3) or *Mki67*$^{-/-}$*Rag1*$^{-/-}$$SW_{HEL}$-$HC^{Ki/Ki}$ (n = 3) mice. Statistical differences were determined by two-tailed unpaired t test with P values shown.

Provided online are three tables. Table S1 shows annotated genes enriched in the GO term cell differentiation GO:0030154. Table S2 shows antibodies used for western blot and flow cytometry. Table S3 shows antibodies and fluorescent dyes used for flow cytometry and cell sorting.